

A hydantoin isoform of cyclic N^6 -threonylcarbamoyladenine (ct^6A) is present in tRNAs

Michał Matuszewski¹, Jakub Wojciechowski², Kenryo Miyauchi³, Zofia Gdaniec⁴, Wojciech M. Wolf², Tsutomu Suzuki^{3,*} and Elzbieta Sochacka^{1,*}

¹Institute of Organic Chemistry, Faculty of Chemistry, Lodz University of Technology, Zeromskiego 116, 90-924 Lodz, Poland, ²Institute of General and Ecological Chemistry, Faculty of Chemistry, Lodz University of Technology, Zeromskiego 116, 90-924 Lodz, Poland, ³Department of Chemistry and Biotechnology, University of Tokyo, 7-3-1 Hongo, Bunkyo-ku, Tokyo 113-8656, Japan and ⁴Institute of Bioorganic Chemistry, Polish Academy of Sciences, Noskowskiego 12/14, 61-704 Poznan, Poland

Received June 22, 2016; Revised November 07, 2016; Editorial Decision November 10, 2016; Accepted November 25, 2016

ABSTRACT

N^6 -Threonylcarbamoyladenine (t^6A) and its derivatives are universally conserved modified nucleosides found at position 37, 3' adjacent to the anticodon in tRNAs responsible for ANN codons. These modifications have pleiotropic functions of tRNAs in decoding and protein synthesis. In certain species of bacteria, fungi, plants and protists, t^6A is further modified to the cyclic t^6A (ct^6A) via dehydration catalyzed by TcdA. This additional modification is involved in efficient decoding of $tRNA^{Lys}$. Previous work indicated that the chemical structure of ct^6A is a cyclic active ester with an oxazolone ring. In this study, we solved the crystal structure of chemically synthesized ct^6A nucleoside. Unexpectedly, we found that the ct^6A adopted a hydantoin isoform rather than an oxazolone isoform, and further showed that the hydantoin isoform of ct^6A was actually present in *Escherichia coli* tRNAs. In addition, we observed that hydantoin ct^6A is susceptible to epimerization under mild alkaline conditions, warning us to avoid conventional deacylation of tRNAs. A hallmark structural feature of this isoform is the twisted arrangement of the hydantoin and adenine rings. Functional roles of ct^6A_{37} in tRNAs should be reconsidered.

INTRODUCTION

Transfer (t) RNA is an adaptor molecule that links the codon in messenger (m) RNA to its corresponding amino acid during protein synthesis. tRNAs contain a number of modified nucleosides that are introduced enzymatically af-

ter transcription. To date, more than 100 species of modified nucleosides have been identified in tRNAs from all domains of life (1). These modifications help to ensure proper tRNA function by stabilizing tertiary structures and modulating decoding properties (2–6). A wide variety of chemical modifications are found in the tRNA anticodon loops, especially at the first letter of the anticodon (position 34), the so-called 'wobble' position. Modifications at this position play critical roles in modulating decoding capabilities (4,6,7). On the other hand, hypermodified purine bases are also found at position 37, 3' adjacent to the anticodon; these modifications contribute to decoding processes by ensuring reading-frame maintenance via stabilization of the codon–anticodon interaction on the ribosome (8,9).

N^6 -Threonylcarbamoyladenine (t^6A) and its derivatives are modifications found at position 37 of tRNAs responsible for decoding A-starting codons (ANN) in all domains of life (Figure 1A) (8,10). Extensive *in vitro* and *in vivo* studies of the biological functions of t^6A revealed that this modification has pleiotropic functions in translation, including aminoacylation of tRNAs (11), tRNA binding to the A-site codon (12), efficient translocation (13), reading-frame maintenance (14) and prevention of leaky scanning of initiation codons and read-through of stop codons (15). Structural studies revealed that t^6A enhances anticodon–codon base pairing by cross-strand base stacking of the t^6A base with the first adenine base of the codon, and stabilizes the anticodon stem–loop structure by stacking with A38 and preventing base-pairing with U33 (16–19).

In 2013, a cyclic form of t^6A (ct^6A) with a molecular mass of 394 Da (Figure 1A) was discovered in bacteria, fungi, protists, and plants (20). Because ct^6A is formed via dehydration of t^6A , it is easily hydrolyzed to t^6A during handling of tRNA and preparation of nucleosides under mild alkali-

*To whom correspondence should be addressed. Tel: +48 42 631 31 55; Fax +48 42 636 55 30; Email: elzbieta.sochacka@p.lodz.pl
Correspondence may also be addressed to Tsutomu Suzuki. Tel: +81 3 5841 8752; Fax: +81 3 5841 0550; Email: ts@chembio.t.u-tokyo.ac.jp

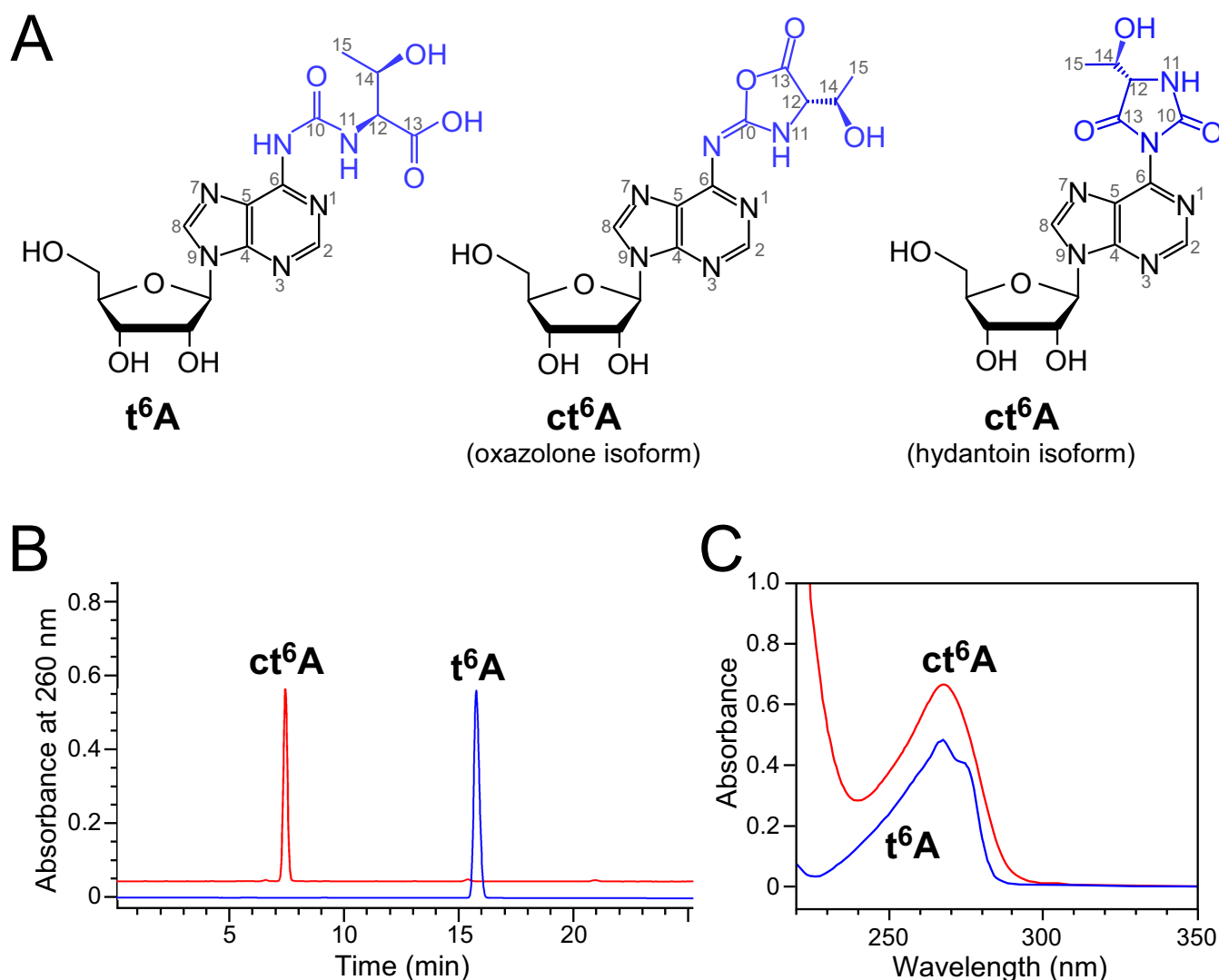


Figure 1. Chemical synthesis of ct⁶A. (A) Chemical structures of t⁶A, oxazolone isoform of cyclic t⁶A, and hydantoin isoform of cyclic t⁶A. (B) HPLC elution profiles of chemically synthesized t⁶A and ct⁶A. (C) UV spectra of chemically synthesized t⁶A and ct⁶A in H₂O; for ct⁶A $\lambda_{\min} = 233$, $\lambda_{\max} = 269$; $\epsilon = 18\,900\text{ dm}^3\cdot\text{mol}^{-1}\cdot\text{cm}^{-1}$.

line conditions (21). Consequently, t⁶A was discovered >40 years (10) before the detection of ct⁶A. When total nucleosides are prepared under neutral conditions in the shortest possible period of time, ct⁶A can be clearly detected, and very little t⁶A is observed in *Escherichia coli* tRNAs (20), demonstrating that ct⁶A is a bona fide modification in tRNAs from species including *E. coli* and yeast. According to MS and NMR analyses, the chemical structure of ct⁶A was determined to be a cyclic active ester with an oxazolone ring (Figure 1A).

ct⁶A is synthesized by tRNA threonylcarbamoyladenine dehydratase A (TcdA), which catalyzes ATP-dependent dehydration of t⁶A to form ct⁶A (20). CsdA and CsdE are additional factors required for efficient ct⁶A formation (20). The yeast homologs of *tcdA*, *TCD1* and *TCD2*, are required for respiratory cell growth, indicating the physiological importance of ct⁶A (20). Reporter assays using a $\Delta tcdA$ strain revealed that ct⁶A is involved in efficient decoding of

tRNA^{Lys}, and possibly for other tRNAs containing ct⁶A. The crystal structures of TcdA in complex with AMP or ATP have been solved (22,23), providing insight into the molecular basis of ct⁶A formation.

The discovery of ct⁶A encouraged us to characterize the structural and biochemical contributions of this modification to tRNA functions. For this purpose, we chemically synthesized the 5',3',2'-*O*-acetylated derivative of ct⁶A, which was stable under acidic and mild basic conditions (24). This advance made it feasible to synthesize model RNA oligonucleotides containing ct⁶A for use in further structural and biochemical studies.

In this study, we elaborated simple synthesis of the non-sugar-protected ct⁶A nucleoside using carbodiimide chemistry, and synthesized ct⁶A nucleoside at multi-milligram scale. The resultant ct⁶A was successfully crystallized, and the tertiary structure of the ct⁶A nucleoside was determined by X-ray crystallography. Contrary to our expecta-

tion, the crystal structure of ct^6A contained a hydantoin isoform rather than the previously determined oxazolone isoform (Figure 1A). These two isoforms are not differentiated by mass spectrometric analysis and simple NMR studies. The hydantoin structure of synthetic ct^6A in solution was further confirmed by detailed analysis of ^{15}N NMR data and the presence of characteristic absorption bands in IR spectrum. Very surprising result of these structural studies prompted us to investigate whether the hydantoin isoform of ct^6A is actually present in natural tRNAs. Careful LC/MS co-injection analysis revealed the identity of the synthetic hydantoin ct^6A with the nucleoside in *E. coli* tRNAs. In addition, we found that hydantoin ct^6A is susceptible to epimerization under mild alkaline conditions, warning us to avoid conventional deacylation procedure of tRNAs. Based on the structural features of this isoform, the structure–function relationship of ct^6A37 in tRNAs should be reconsidered.

MATERIALS AND METHODS

General information

A Waters HPLC (515) system using XTerra[®] Waters column (MS C8, 5 μ m, 4.6 \times 150 mm, 100 Å) was used for analytical high-performance liquid column chromatography (HPLC). Chromatography was performed at room temperature, at a flow rate of 1 ml/min, in a gradient of acetonitrile (Solvent B) in 0.1% AcOH/water (Solvent A), as follows: 0% B to 30% B in 0–30 min, and 30% B to 50% B in 30–35 min. The elution profile was monitored by UV absorption at 254 nm using a Waters 996 photodiode array detector. High-resolution mass spectrometry with electrospray ionization was conducted on a Maldi SYNAPT G2-S HDMS (Waters). UV-vis spectra were obtained on an O-2800 Hitachi UV Digilab1 spectrophotometer. IR data were recorded on an FT-IR ALPHA (Bruker) equipped with a Platinum ATR QuickSnap[™] module. NMR spectra were recorded in DMSO- d_6 on Bruker Avance II Plus 700 and Bruker DPX-250 spectrometers. Chemical shifts are given as ppm values relative to DMSO, used as an internal reference (2.50 ppm for 1H NMR and 39.51 ppm for ^{13}C NMR). Signals were assigned based on 1H - 1H COSY, 1H - ^{13}C HSQC, 1H - ^{13}C HMBC and ^{13}C DEPT 135 spectra. Signals shapes and multiplicities are indicated as follows: br s = broad singlet, s = singlet, d = doublet, dd = double doublets, ddd = double double doublets, t = triplet, q = quartet, m = multiplet. Scalar coupling constants J are given in Hertz (Hz). ^{15}N chemical shifts were obtained from analysis of 1H - ^{15}N HSQC and 1H - ^{15}N HMBC spectra, and are given relative to liquid NH_3 . 1D NOE and 2D NOESY spectra were recorded with a mixing time of 300 ms.

Chemical synthesis of t^6A

t^6A nucleoside was obtained in good yield according to the procedure reported by Chheda *et al.* (25–27). In this method, the exo-amine group of sugar-acetylated adenosine was functionalized with an ethoxycarbonyl group using ethylchloroformate as the electrophile, affording a reactive N^6 -carbamate derivative. The ethoxy group of this compound was subsequently substituted with L-threonine to

give sugar-protected t^6A , which was de-protected by treatment with ammonium-saturated methanol (10 M), yielding the t^6A nucleoside as the ammonium salt. The t^6A ammonium salt was then purified by column chromatography on silica gel 60 (230–400 mesh, Sigma-Aldrich). Before cyclization, the t^6A ammonium salt was converted to the nucleoside with a free carboxylate by cation ion exchange chromatography on Amberlite[™] IR120 (H^+ form). The purity and structure of the t^6A nucleoside were unambiguously confirmed by analytical HPLC (Figure 1B), UV spectrum (Figure 1C), IR (Supplementary Figure S1A), 1H NMR (Supplementary Figure S2A) and ^{13}C NMR (Supplementary Figure S3A), and the results were in full agreement with earlier publications (25–28).

t^6A nucleoside bearing D-*allo*-threonine residue was synthesized according to the same procedure as described above for L- t^6A isomer. The spectral data of D-*allo*- t^6A fully correlated with those reported previously (29), and they are shown in Supplementary Figure S4A (IR), Supplementary Figure S5A (1H NMR) and Supplementary Figure S6A (^{13}C NMR).

Chemical synthesis of ct^6A

t^6A nucleoside in the free carboxylic form (300 mg, 0.72 mmol) was dissolved in 10 ml of water and mixed with 1-ethyl-3-(3-dimethylaminopropyl)-carbodiimide immobilized on a polymer support (EDC-P) (10 equiv, 5.14 g, 7.2 mmol, loading 1.4 mmol/g), followed by vigorous stirring at room temperature for 1 h. After consumption of t^6A nucleoside was checked by TLC analysis (*n*-BuOH/ H_2O = 85/15, v/v), the reaction was quenched by filtering off the polymer-bounded EDC, followed by three careful washes of the polymer bed with H_2O (10 ml each time). The filtrate was evaporated to dryness under reduced pressure, and the crude product was subjected to column chromatography on silica gel with a linear gradient of H_2O (0–3%) in *n*-BuOH to purify ct^6A nucleoside (140 mg, yield 49%). ct^6A nucleoside was obtained with similar yield (153 mg, yield 51%) using dimethylformamide (DMF) as a solvent. The purity of ct^6A and its different lipophilicity relative to t^6A was confirmed by analytical HPLC (Figure 1B), UV spectroscopy (Figure 1C), IR (Supplementary Figure S1B), 1H NMR (Supplementary Figure S2B), ^{13}C NMR (Supplementary Figure S3B), and high-resolution MS (Supplementary Figure S7).

Cyclization of D-*allo*- t^6A was performed with the same procedure as described above to generate D-*allo*- ct^6A with slightly lower yield (40%). The structure of D-*allo*- ct^6A was confirmed by IR (Supplementary Figure S4B), 1H NMR (Supplementary Figure S5B) and ^{13}C NMR (Supplementary Figure S6B). HPLC co-injection analysis of D-*allo*- ct^6A and L- ct^6A mixture showed that both isomers can be clearly separated (Supplementary Figure S8).

Single crystal X-ray diffraction analysis

Colorless crystals of ct^6A (0.30 \times 0.10 \times 0.05 mm) were obtained from aqueous ethanol (1:1) solution. Single crystal X-ray diffraction data were collected on a Bruker Smart APEX2 diffractometer at 100 K, using an Incoatec Microfocus Source $I\mu$ S Cu- $K\alpha$ (λ = 1.54178 Å) as the source of ra-

diation. Integration of the data yielded 14 087 reflections to a $2\theta_{\max}$ angle of 142° , of which 3384 were independent ($R_{\text{int}} = 0.040$), and 3152 reflections with $I \geq 2\sigma(I)$. The crystal structure was solved by the intrinsic phasing method. Formula: $\text{C}_{15}\text{H}_{18}\text{N}_6\text{O}_7 \cdot \text{H}_2\text{O}$, $M_w = 412.37$, $Z = 4$, crystal system: orthorhombic, space group: $P2_12_12_1$, $a = 6.355(1)$, $b = 8.173(1)$, $c = 33.492(3)$ Å, $\alpha = \beta = \gamma = 90^\circ$, $V = 1739.4(2)$ Å³, $\rho_{\text{calcd}} = 1.57$ g cm⁻³, $\mu = 1.11$ mm⁻¹. Semi-empirical absorption correction based on multiple scanned equivalent reflections ($0.636 < T < 0.754$) was applied. The final anisotropic full-matrix least-squares refinement on F^2 with 342 variables converged at $R_{\text{obs}} = 0.041$, $R_{\text{all}} = 0.045$, $wR(F^2) = 0.099$ with residual electron density $\Delta\rho_{\text{max}} = 0.23$ eÅ⁻³ ($\Delta\rho_{\text{min}} = -0.25$ eÅ⁻³). Positions of all hydrogen atoms were located on a difference Fourier map, and their coordinates and isotropic displacement parameters were refined without restriction, with the exception of hydrogen atoms in water molecules, whose parameters were restrained to the oxygen atom. The correct absolute configuration was provided using a starting material with known configuration. Data collection, reduction, and absorption correction were performed using the APEX2 (Version 2014.9, Bruker AXS), SAINT-PLUS (Version 8.34A, Bruker AXS), and SADABS (Version 2014/4, Bruker AXS) programs, respectively. Structure solution and refinement were performed using the SHELXTL suite (Version 2014/6, Bruker AXS). The CDCC 2015 software package (CSD system 2015, Version 5.36, Conquest, Mercury, Mogul) (30) was utilized for subsequent molecular geometry analysis and visualizations.

Quantum chemistry computations

Ab initio energy scans around N1-C6-N6-C13 torsion angle for ct⁶A were performed using the Gaussian09 program with the DFT methodology (Gaussian 09, Revision C.01, Gaussian, Inc., Wallingford CT, 2010). The Truhlar exchange-correlation energy functional M062x and aug-cc-pvdz Dunning's basis set were applied to calculate the wave functions. Initial atomic coordinates were those determined for the crystal. For rigid energy scans, a 10° step was set, and then for every conformer an EM062x was computed without molecular geometry optimization. Differences in energies (ΔE) compared to E_{M062x} for the initial atomic coordinates were calculated, and their highest values are defined as energies of the rotation barrier. For relaxed energy scans, the geometric parameter under investigation was set to a starting value and then iteratively increased by 20° . For each scan step, the optimized molecular geometry E_{M062x} was calculated. Conformational energy (ΔE) was calculated as the difference between the particular conformer E_{M062x} and the lowest value of E_{M062x} determined during the energy scan.

Nucleoside analysis by mass spectrometry

Total RNA was extracted from *E. coli* strain BW25113 cultured in LB broth for 18 h, using the acidic phenol method as reported previously (20). Total nucleosides were prepared by digesting *E. coli* total RNA with nuclease P1 (Wako Pure Chemical Industries) and bacterial alkaline phosphatase (BAP) (*E. coli* strain C75, TAKARA BIO INC.) under acidic conditions (31). For these reactions, a

solution (typically 40 μl) containing 1 $\mu\text{g}/\mu\text{l}$ total RNA, 20 mM trimethylamine-acetate (pH 5.3), nuclease P1 (0.1 units for 40 μg of RNA), and BAP (0.16 units for 40 μg of RNA) was incubated at 37°C for 1 h.

Total nucleosides were analyzed using a Q Exactive hybrid Quadrupole-Orbitrap mass spectrometer (Thermo Fisher Scientific) equipped with an ESI source and Ultimate 3000 liquid chromatography system (Dionex). For HILIC/ESI-MS (31) was performed using a ZIC-cHILIC column (3 μm particle size, 2.1×150 mm, Merck Millipore). The mobile phase consisted of 5 mM ammonium acetate (pH 5.3) (solvent A) and acetonitrile (solvent B). Total nucleosides (2 μg) or synthetic ct⁶A (5 pmol) dissolved in 90% acetonitrile were injected and chromatographed with a flow rate of 100 $\mu\text{l}/\text{min}$ in a multistep linear gradient: 90–40% B from 0 to 30 min, 40% B for 10 min, followed by initialization to 90% B. Proton adducts of nucleosides were scanned in positive polarity mode over an m/z range of 110–700. ODS/ESI-MS (32) was performed on a Sunshell C18 column (2.6 μm particle size, 2.1×150 mm, ChromaNik Technologies) with the same solvent system described above. The gradient program was as follows: 0–40% B from 0 to 30 min, 40% B for 5 min, followed by initialization to 0% B, at a flow rate of 75 $\mu\text{l}/\text{min}$. Total nucleosides (4 μg) or synthetic ct⁶A (10 pmol) dissolved in LC/MS grade ultrapure water (Wako) were injected. Positively charged nucleosides were scanned over an m/z range of 200–500. For higher-energy collision-induced dissociation (CID) in ODS/ESI-MS, the following gradient program was used: 0–15% B from 0 to 30 min with a curved gradient, 15–60% B from 30 to 35 min, 60% B for 10 min, followed by initialization to 0% B, at a flow rate of 75 $\mu\text{l}/\text{min}$. Bases liberated from nucleosides by in-source fragmentation (20 eV) were scanned over an m/z range of 240–400, and further scanned by data-dependent HCD with a normalized collision energy of 30. Total nucleosides (12 μg) or synthetic ct⁶A (400 pmol) dissolved in LC/MS grade ultrapure water were subjected to this analysis.

Epimerization of ct⁶A

For synthetic nucleosides, 4 nmol of L-ct⁶A or D-*allo*-ct⁶A was dissolved in 400 μl of 100 mM sodium borate buffer (pH 9.0) and incubated at 37°C for 5 min, followed by adding 10 μl of 3 M NaOAc (pH 5.2) to stop the reaction. The nucleosides were desalted by using Oasis HLB cartridge (3 ml, 30 mg, Waters), dried *in vacuo* and dissolved in water. 10 pmol of each sample was subjected to ODS/ESI-MS as described above.

For natural ct⁶A, 160 μg of *E. coli* total RNA in 400 μl of 100 mM sodium borate buffer (pH 9.0) was incubated at 37°C for 15 min, followed by adding 40 μl of 3 M NaOAc (pH 5.2) to stop the reaction and subjected to ethanol precipitation to recover total RNA. Nucleoside preparation was carried out by one-step acidic digestion (31) as described above. Four microgram of total nucleoside was subjected to ODS/ESI-MS. For co-injection analysis, 10 pmol of D-*allo*-ct⁶A was mixed.

For amine adduct formation, 4 nmol of L-ct⁶A or D-*allo*-ct⁶A, or 160 μg of *E. coli* total RNA was dissolved in 400 μl of 100 mM Tris-HCl (pH 8.5) and incubated at 37°C for 3 h.

Further preparation was performed as the same procedure described above.

RESULTS

Chemical synthesis of ct⁶A

As reported previously (24), 5',3',2'-*O*-acetylated derivative of L-ct⁶A was synthesized by dehydration of sugar protected L-t⁶A with acetic anhydride, while for L-ct⁶A preparation carbodiimide chemistry was applied (20). Here, for multi-milligram scale synthesis, we used polymer-bound EDC as the activating agent for the carboxyl group of t⁶A. After the reaction, the polymer-bound EDC and its urea form product were removed by filtration, and the product was separated by silica gel column chromatography. The purity of the products was confirmed by HPLC analysis (Figure 1B). Yields of L-ct⁶A nucleoside synthesized in water and DMF as solvents were 49% and 51%, respectively. The resultant L-ct⁶A nucleoside was characterized by UV (Figure 1C), IR (Supplementary Figure S1B), ¹H NMR (Supplementary Figure S2B), ¹³C NMR (Supplementary Figure S3B) and MS (Supplementary Figure S7); the results were identical to those reported previously (20).

We also synthesized diastereoisomer of ct⁶A with *D*-allo-threonine (C α epimer) to examine possible epimerization of L-ct⁶A under mild alkaline conditions. First, we obtained *D*-allo-t⁶A nucleoside that was subjected to the cyclization with the same procedure as for L-ct⁶A nucleoside. The resultant *D*-allo-ct⁶A nucleoside was characterized by IR (Supplementary Figure S4B), ¹H NMR (Supplementary Figure S5B) and ¹³C NMR (Supplementary Figure S6B). L-ct⁶A and *D*-allo-ct⁶A nucleosides were clearly separated by HPLC analysis (Supplementary Figure S8).

Hydantoin isoform of ct⁶A revealed by crystal structure

The ct⁶A nucleoside crystallized as the monohydrate in an orthorhombic crystal system of space group *P*2₁2₁2₁. Additional X-ray crystallography data are summarized in Supplementary Tables S1–S5. Strikingly, the crystal structure showed that the N⁶-substituent of ct⁶A adopts the hydantoin form (Figure 2A), rather than the previously assigned oxazolone form (Figure 1A). This observation prompted us to check whether the isomerization occurs during the crystallization. However, careful analysis of ct⁶A nucleoside by TLC and HPLC before and after crystallization (data not shown) revealed that no isomerization occurred during this process.

In this structure, the hydrogen bonds between molecules play a vital role in crystal packing (Supplementary Table S6). In particular, the N3 nitrogen forms a strong intermolecular bond with 5'-OH in the ribose, stabilizing the *syn* conformation of the ct⁶A base (Figure 2A). The water molecule localized in the crystal links O3' of the ribose and O10 in the hydantoin ring from another molecule. These interactions enable formation of unique crystal packing with an infinite layer of sugar rings perpendicular to the [001] direction (Figure 2B).

Detailed structure of hydantoin ct⁶A

The bond lengths and valency angles in the adenosine and hydantoin moieties of ct⁶A (Supplementary Tables S3 and S4) are consistent with the respective values observed in crystal structures of similar chemical compounds deposited in the Cambridge Structural Database (CSD) (Supplementary Table S5) (30). The only significant difference in the ct⁶A nucleoside is the C6–N6 bond, which is longer (1.407(4) Å) than the corresponding bond in the structure of t⁶A nucleoside (1.3784(3) Å). This difference can be explained by repulsive interactions between the carbonyl oxygens of the ct⁶A hydantoin ring and the N1 and N7 nitrogens of the adenine moiety (Figure 1A). Similarly, elongated C6–N6 bond (1.413 Å) was found in the crystal structure of adenyln⁶-tetramethylsuccinimide (CSD-PULQIX), a modified adenosine with a cyclic imide containing the N6 nitrogen (33).

The ureido functionality in the ct⁶A hydantoin ring exhibits a significant electron density delocalization (Supplementary Figure S9). The elongated C10–N6 bond (1.428(4) Å) accompanied by the short C10–N11 bond (1.337(5) Å) (Supplementary Table S3) indicate a possibility of tautomeric conversion to the enol form with protonation at O10, which is additionally stabilized by hydrogen bonding with a nearby water molecule. Similarly, in the t⁶A structure, the ureido group is also influenced by electron density delocalization as indicated by relatively long C10–N6 (1.4089(3) Å) and short C10–N11 (1.3216(3) Å) bonds (34,35).

The relative orientation of the hydantoin and adenine rings in the ct⁶A crystal structure is described by the η (N1–C6–N6–C13) dihedral angle. It adopts value of $-52.7(5)^\circ$, clearly indicating twisting arrangement of those rings (Figure 2A and Table 1). It is stabilized by the repulsive interactions between carbonyl oxygens of the hydantoin ring and the N1 and N7 nitrogens of the adenine moiety (Supplementary Figure S9). This repulsion restricts free rotation around C6–N6 bond. Indeed, an *ab initio* energy rigid scan over the η angle revealed two rotation barriers around $\eta = 0^\circ$ ($\Delta E = 23.0$ kcal) and $\eta = 180^\circ$ ($\Delta E = 17.7$ kcal) arising from the plane arrangement of these two rings (Figure 3). The dihedral angle $\eta = -52.7(5)^\circ$ observed in the crystal is close to the most stable conformation determined by the rigid energy scans (Figure 3). Similar rotation barriers were also observed by the relaxed energy scan (Supplementary Figure S10). The corresponding twisted arrangement of two rings was found in the crystal structure of adenyln⁶-tetramethylsuccinimide (CSD-PULQIX) with a corresponding dihedral angle $\eta = -43.3^\circ$ (33).

The ribose of ct⁶A adopts the C2'-*endo* pucker conformation (Figure 2A) with the values of endocyclic torsion angles $\nu_0 - \nu_4$ shown in Table 1. The pseudorotation phase angle and puckering amplitude (36,37) are $P = 160.9(3)^\circ$ and $\tau_m = 37.2(2)^\circ$, respectively. Because the torsion angle about the C4'–O4' bond is only 0.4° , the conformation of the ribose moiety is almost exactly ²E. Similar sugar ring puckering was also observed in the t⁶A crystal structure, with $P = 157.8^\circ$ and $\tau_m = 31.8^\circ$ (35).

Conformation of the 5'-hydroxymethyl group of the ct⁶A nucleoside is described by the dihedral angle γ and $\gamma(-)$ (37) and their values (Table 1) define a *gauche*(+) conformation

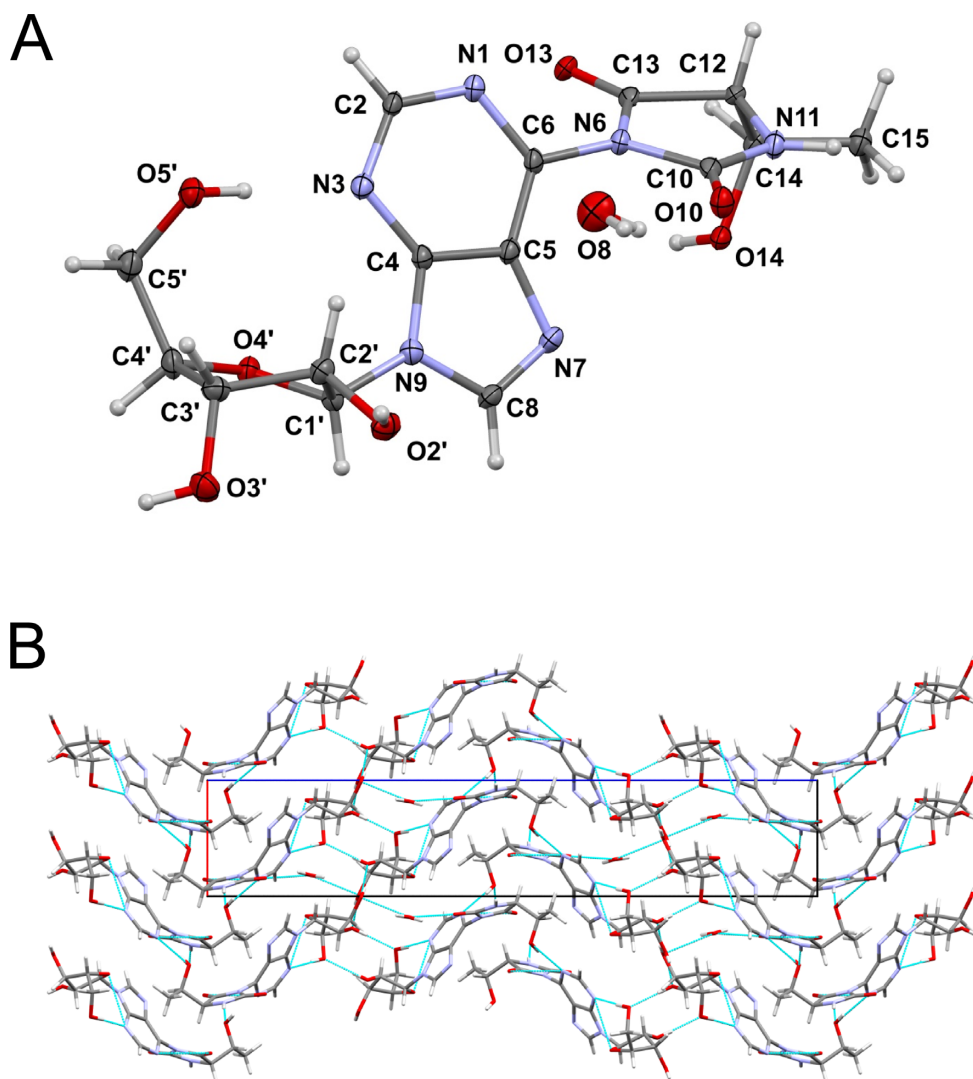


Figure 2. Crystal structure of chemically synthesized ct⁶A. (A) Crystal structure of the hydantoin isoform of ct⁶A. Displacement ellipsoids were drawn at the 50% probability level. Hydrogen atoms are represented by circles with an arbitrary radius. (B) Crystal packing of ct⁶A. Hydrogen bonds are indicated by dashed blue lines.

Table 1. Selected dihedral angles (°) of ct⁶A and t⁶A

Dihedral angles	ct ⁶ A	t ⁶ A
N6 substituent arrangement		
N1–C6–N6–C13 (η)	– 52.7(5)	– 1.54(5)
Nucleoside conformation		
C4'–O4'–C1'–C2' (ν_0)	– 23.1(4)	– 21.31(5)
O4'–C1'–C2'–C3' (ν_1)	35.9(3)	31.72(5)
C1'–C2'–C3'–C4' (ν_2)	– 34.1(3)	– 29.49(5)
C2'–C3'–C4'–O4' (ν_3)	22.0(4)	17.99(5)
C3'–C4'–O4'–C1' (ν_4)	0.4(4)	1.95(5)
O5'–C5'–C4'–C3' (γ)	48.4(4)	57.23(5)
O5'–C5'–C4'–O4' (γ^-)	– 71.0(4)	– 63.76(5)
C4'–N9–C1'–O4' (χ)	51.0(4)	– 153.41(5)

around the exocyclic C4'–C5' bond. Similar conformation was also found in the t⁶A crystal structure (35).

The glycosidic dihedral angle $\chi = 51.0(4)^\circ$ (Table 1) clearly indicates the *syn* conformation of the ct⁶A base. It is stabilized by the intramolecular hydrogen bond between

5'OH of sugar moiety and N3 nitrogen of heterobase. This type of interaction has not been found in crystal structure of the t⁶A nucleoside which adopts the *anti* conformation around the N-glycosidic bond (35).

Spectroscopic characterization of ct⁶A

The ct⁶A nucleoside was further characterized by NMR spectroscopy. All ¹H and ¹³C resonances of ct⁶A were unambiguously assigned by a combination of ¹H, ¹H-COSY, ¹H, ¹H-NOESY, ¹H, ¹³C-HSQC and ¹H, ¹³C-HMBC experiments, all of which are identical to our published data (20). However, these NMR analyses did not provide direct evidence allowing differentiation of the two isoforms of ct⁶A. To obtain a signature of the hydantoin isoform of ct⁶A, we further recorded ¹H, ¹⁵N-HSQC and ¹H, ¹⁵N-HMBC spectra for the ct⁶A nucleoside to determine ¹⁵N chemical shifts (Table 2 and Supplementary Figure S11). The chemical shifts of N6 (163 ppm) and N11 (87 ppm) of ct⁶A were in

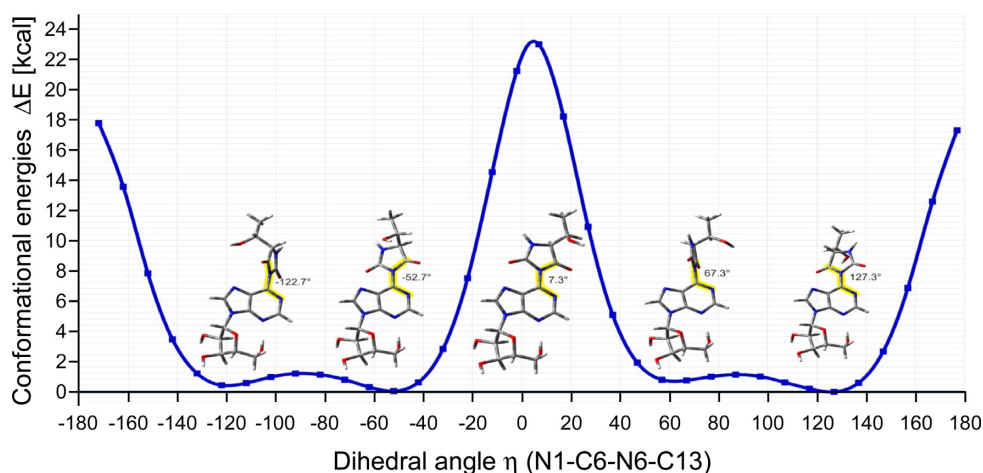


Figure 3. *Ab initio* energy calculation for the rigid scan over the dihedral angle η . The rigid energy scan over the dihedral angle η (N1–C6–N6–C13) was performed at 10° steps using the hybrid functional M062x and aug-cc-pvdz Dunning's basis set. Initial atomic coordinates were obtained from the crystal structure. ΔE is calculated as the E_{M062x} difference between the coordinates of each conformer and the initial coordinates. Structural models of ct^6A are depicted at the indicated η angles.

Table 2. ^{15}N chemical shifts of ct^6A and t^6A in DMSO

	ct^6A	t^6A
N-1	275	233
N-3	254	236
N-7	241	239
N-9	171	172
N-6	163	116
N-11	87	93

^{15}N chemical shifts (ppm) relative to liquid NH_3 .

the range characteristic to urea-type nitrogens, consistent with the analogous nitrogens in the N^3 -phenyl hydantoin structure (38), supporting the idea that the hydantoin isoform actually exists in solution. In the case of the oxazolone isoform, the C=N–Ar type nitrogen would appear at much lower magnetic field (39).

We next obtained IR spectra of t^6A (Supplementary Figure S1A) and ct^6A (Supplementary Figure S1B). The characteristic ureido carbonyl absorption at 1680 cm^{-1} in t^6A disappeared in the spectrum of ct^6A , and was replaced by two absorption bands at 1780 and 1730 cm^{-1} . These absorptions are in the same range as the hydantoin ring of 3-purin-6-yl-hydantoin (40), further supporting the idea that the synthetic ct^6A adopts the hydantoin isoform.

Solution structure of hydantoin ct^6A

Conformation of hydantoin ct^6A in solution was determined using NMR spectroscopy. The conformation of the ribose was inferred by vicinal spin–spin coupling constants determined by 1H NMR spectra in D_2O (Supplementary Figure S12). At room temperature, the C2'-*endo* and C3'-*endo* conformers of ct^6A were equally populated in solution, while in the crystal it was C2'-*endo* sugar pucker (Figure 2A). Regarding exocyclic C4'–C5' bond, we found that *gauche* (+) is the preferred conformation ($\sim 62\%$) of ct^6A in solution which is consistent with the result of the crystal structure.

Then, we conducted 1D NOE experiments to examine orientation of the ct^6A base relative to the ribose (41,42). When H8 was irradiated, strong NOE effect was observed to H2' rather than to H1' (Supplementary Figure S13 and Supplementary Table S7), suggesting that ct^6A predominantly takes *anti* conformation in solution. Supporting this finding, a strong cross peak of H8–H2', and a weak cross peak of H8–H1' were also observed in 2D NOESY spectrum in D_2O (Supplementary Figure S14). All of these results confirmed the *anti* conformation of ct^6A . This observation is not consistent with that found in the crystal structure where the ct^6A base adopts the *syn* conformation. The relative orientation of the hydantoin and adenine rings could not be provided by NMR data analyses as there are no vicinal coupling constants available for the Karplus-like relationship.

Presence of hydantoin ct^6A in *E. coli* tRNAs

To determine whether the hydantoin isoform of ct^6A is actually present in cellular tRNAs, we conducted LC/MS analyses to compare synthetic and natural ct^6A . In reverse-phase column chromatography (ODS) coupled with mass spectrometry, the synthetic ct^6A and natural ct^6A in total nucleosides in *E. coli* tRNAs eluted at similar retention times, ~ 24 min (Figure 4A). When both specimens were co-injected, we observed a single peak of mass chromatogram at m/z 394 (Figure 4A). In addition, we conducted the same MS analysis using hydrophilic interaction chromatography (HILIC). The synthetic and natural ct^6A co-eluted at the same retention time as well (Figure 4B).

Next, we performed higher-energy collision-induced dissociation (CID) analysis of the base-related ion (BH^{2+}) of both synthetic and natural ct^6A . Product ions generated from the BH^{2+} of ct^6A (m/z 263) were almost identical for both specimens (Figure 5A and B). These product ions could be assigned in the chemical structure of the hydantoin isoform of the ct^6A base (Figure 5C).

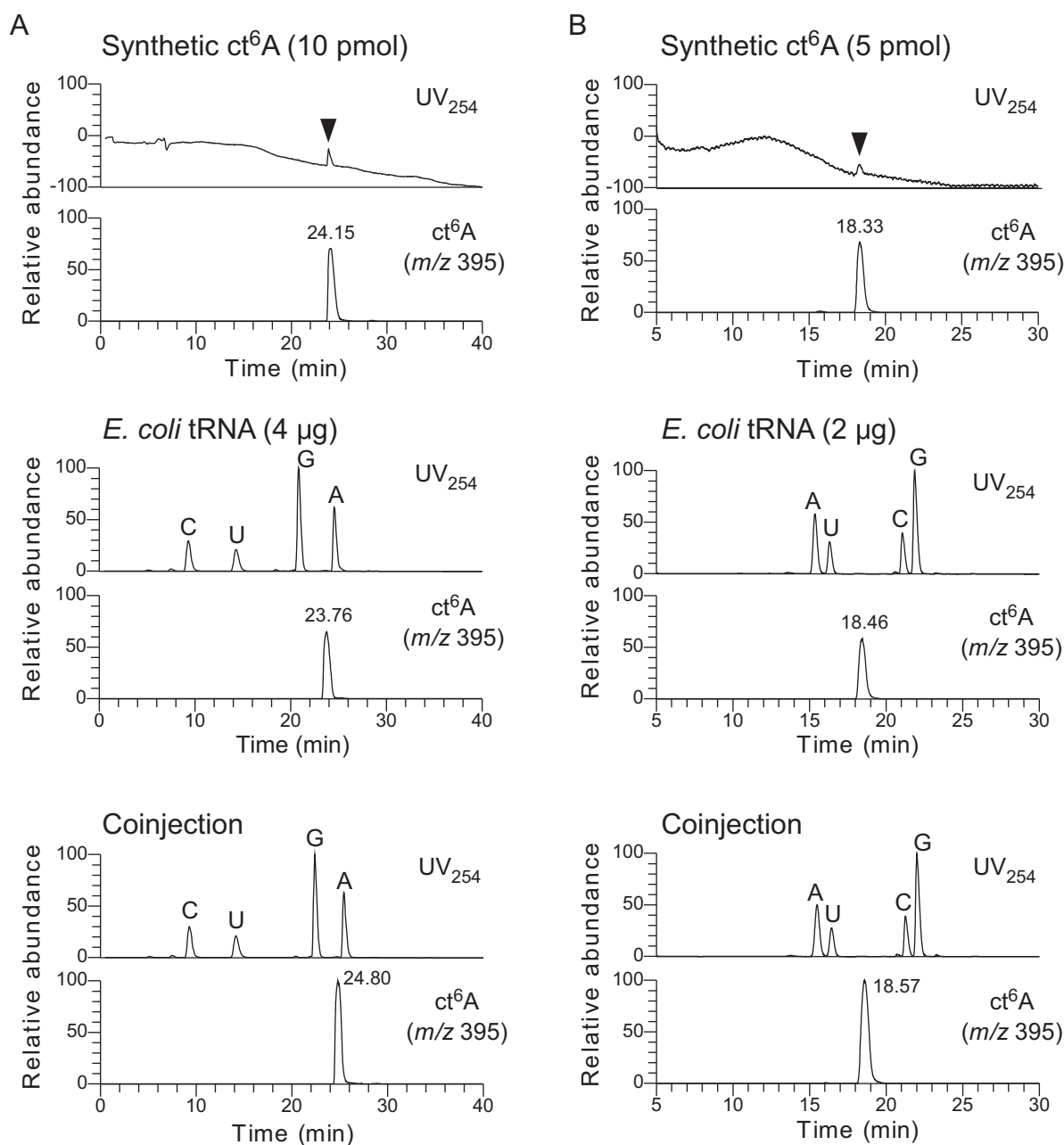


Figure 4. LC/MS co-injection analyses of synthetic and natural ct^6A nucleosides. LC/MS analyses of synthetic ct^6A and *E. coli* total nucleosides by reverse-phase chromatography using octadecylsilyl resin (ODS, **A**), and by hydrophilic interaction chromatography (HILIC, **B**). UV traces (254 nm) and mass chromatograms (m/z 395) of synthetic ct^6A (top), natural ct^6A in *E. coli* total RNA (middle), and co-injected natural and synthetic ct^6A (bottom). ct^6A peaks in the UV trace are indicated by arrows.

Epimerization of hydantoin ct^6A under mild alkaline conditions

When total RNA was digested into nucleosides by conventional condition (pH 8.2), most of ct^6A was hydrolyzed and converted to t^6A as reported (20). In this condition, we noticed appearance of second peak of t^6A that elutes faster than the original peak of t^6A in LC/MS chromatogram (20). In addition, rest of ct^6A also split and gave second peak that elutes slower than the original ct^6A peak (20). When ct^6A was incubated with Tris buffer, two peaks of

Tris-adduct of t^6A appeared (20). These findings prompted us to speculate that α -carbon of threonine residue in hydantoin ring is epimerized under mild alkaline treatment (Supplementary Figure S15). To confirm this speculation, ct^6A epimer (*D-allo-ct^6A*) was synthesized chemically, and compared to *L-ct^6A* treated under mild alkaline condition and/or incubated with Tris buffer. As shown in Figure 6A, the synthetic *L-ct^6A* gave a single peak in LC/MS. In addition, *L-t^6A*, a hydrolyzed product of *L-ct^6A*, was also detected. When *L-ct^6A* was incubated with a buffer adjusted at pH 9 for 5 min, second peak of ct^6A that eluted slower

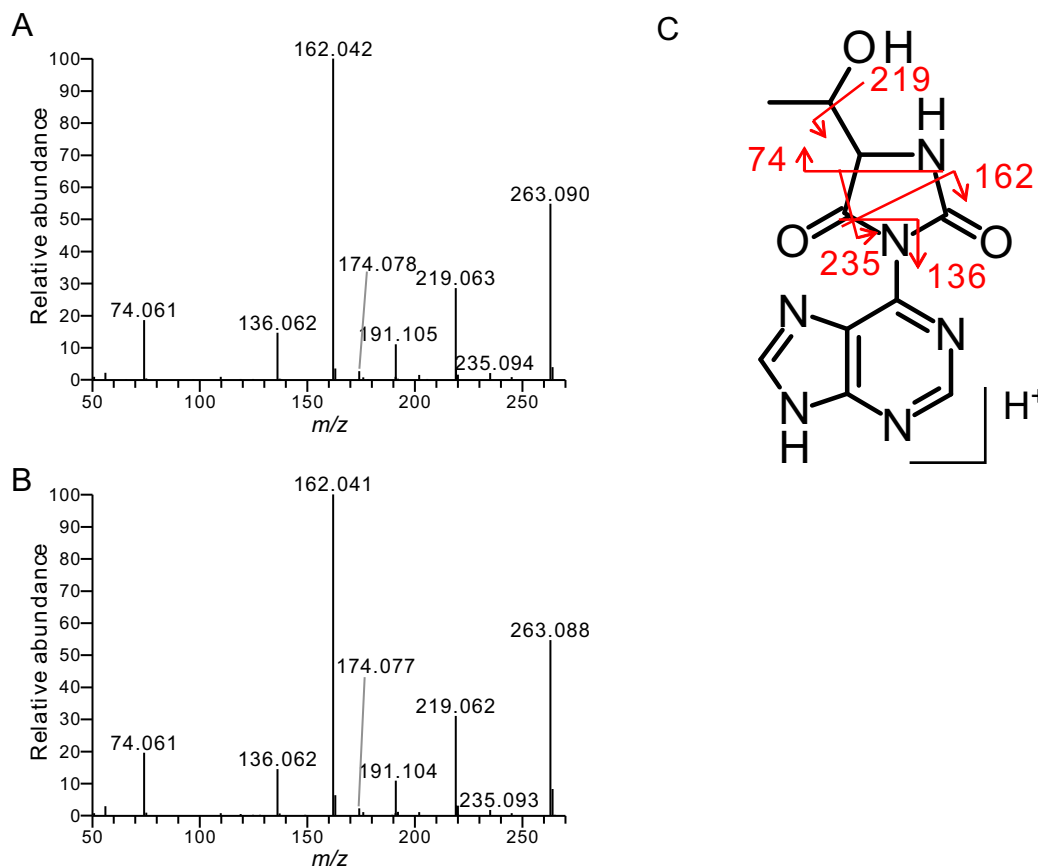


Figure 5. CID spectra of the ct^6A base. CID spectra of the ct^6A base (m/z 263) derived from synthetic ct^6A nucleoside (A) and *E. coli* total nucleosides (B). (C) Product ions are assigned in the chemical structure of the hydantoin isoform of the ct^6A base.

than the L- ct^6A peak clearly appeared, while second peak of t^6A that eluted faster than the L- t^6A peak was also detected. Judging from the retention times of the synthetic D- $allo-ct^6A$ and its hydrolysate, D- $allo-t^6A$, these second peaks were found to be D- $allo-ct^6A$ and D- $allo-t^6A$, respectively (Figures 6A and Supplementary Figure S15). Furthermore, when the synthetic D- $allo-ct^6A$ was incubated under mild alkaline conditions (pH 9 for 5 min), L- ct^6A and L- t^6A clearly appeared. To confirm these findings, L- ct^6A treated with mild alkaline was coinjected with D- $allo-ct^6A$ which was treated or untreated with mild alkaline (Supplementary Figure S16). Second peaks of L- ct^6A appeared under mild alkaline conditions coeluted with D- $allo-ct^6A$ and D- $allo-t^6A$, respectively.

Next we examined epimerization of natural ct^6A in *E. coli* tRNAs. As reported previously (20), when *E. coli* total RNA was incubated with a buffer at pH 9 for 15 min, we detected D- $allo-ct^6A$ along with D- $allo-t^6A$ (Figure 6B). D- $allo-ct^6A$ in *E. coli* total RNA was confirmed by coinjection with synthetic specimen. Moreover, we examined epimerization of t^6A upon adduct formation with amine. When the synthetic or natural ct^6A was incubated with Tris buffer at pH 8.5, both L-type and D- $allo$ -type Tris adducts of t^6A were generated (Figure 6C).

Collectively, these findings demonstrate that epimerization of ct^6A takes place under alkaline conditions, even at

pH 8.5, followed by epimer formation of t^6A and its amine-adducts.

DISCUSSION

The crystal structure of the ct^6A nucleoside clearly demonstrates that ct^6A adopts a hydantoin isoform (Figure 2A), rather than the previously predicted oxazolone isoform (20). We also confirmed that the hydantoin ct^6A is actually present in *E. coli* tRNAs (Figure 4). As shown here, it was impossible to differentiate the two isoforms by a series of NMR and MS analyses, explaining the reason why the chemical structure of ct^6A was once assigned to be the oxazolone isoform. For instance, the product ions of CID spectrum of ct^6A base (Figure 5A and B) could be assigned to the hydantoin isoform as well as to oxazolone isoform (Supplementary Figure S17) (20). Additionally, a pattern of the scalar couplings observed in $^1H-^1H$ -COSY spectra of both isoforms is very similar. In $^1H-^1H$ -COSY spectrum of ct^6A , we observed cross peaks between NH11–H12, H12–H14, H14–OH14 and H14–H15 attributed to the threonine side chain (Supplementary Figure S18), however, these couplings are present in both hydantoin and oxazolone isoforms. No coupling was found between amino acid side chain and adenine base. In this study, however, we have found three spectroscopic features implying the presence of a hydantoin group in ct^6A . First, the unique chemical shift

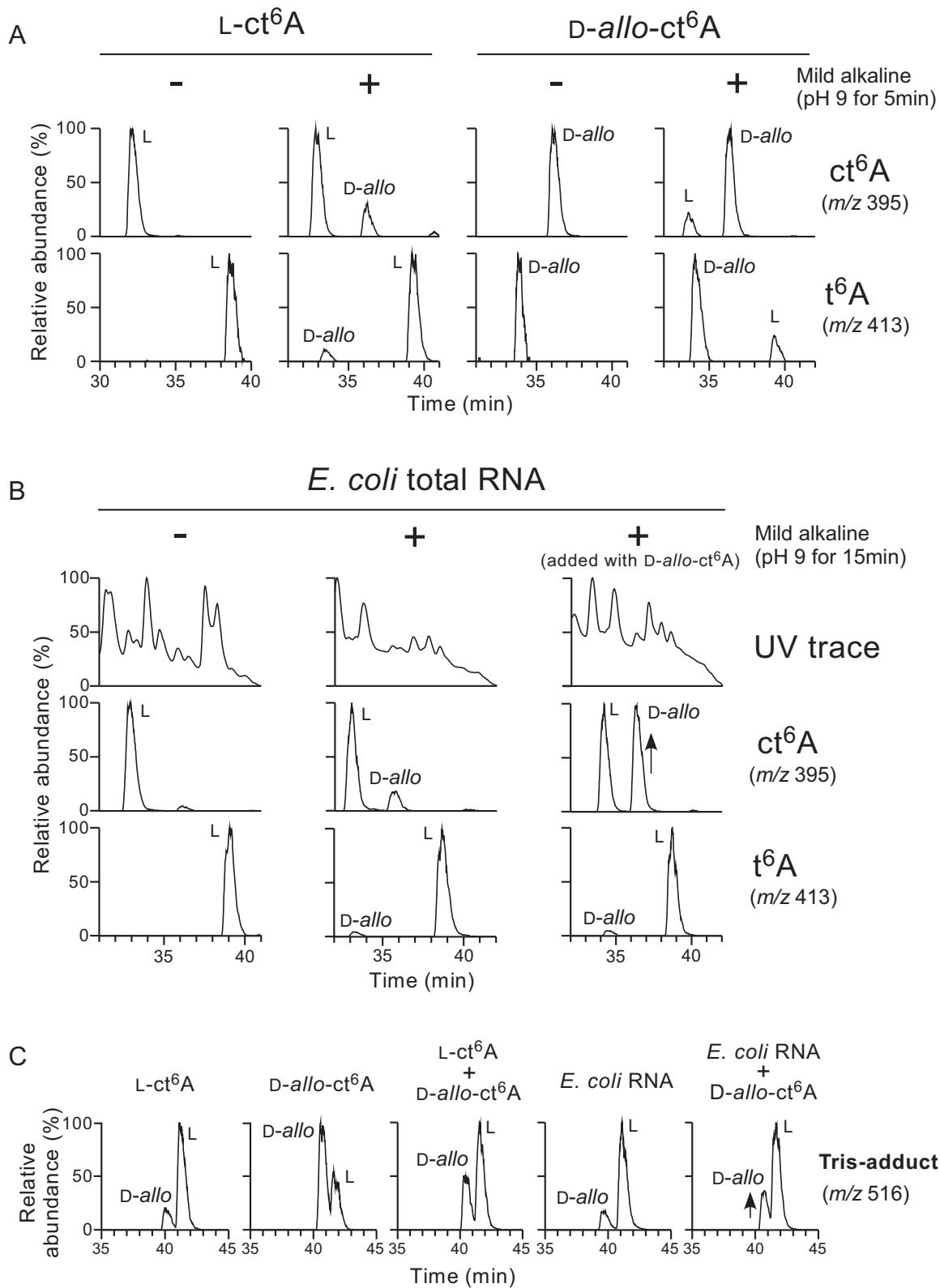


Figure 6. Epimerization of ct⁶A. (A) Epimerization of synthetic L-ct⁶A and D-allo-ct⁶A under mild alkaline condition. Each nucleoside was treated with (+) or without (–) mild alkaline (pH 9 for 5 min), and subjected to ODS/ESI-MS analysis to detect ct⁶A (*m/z* 395, upper panels) and t⁶A (*m/z* 413, lower panels). A peak corresponding to each epimer is indicated in the chromatographs. (B) Epimerization of natural ct⁶A in *E. coli* total RNA under mild alkaline condition. *E. coli* total RNA was treated with (+) or without (–) mild alkaline (pH 9 for 15 min), digested into nucleoside under acidic condition, and subjected to ODS/ESI-MS analysis to detect UV trace at 254 nm (top panels), ct⁶A (*m/z* 395, middle panels) and t⁶A (*m/z* 413, bottom panels). (C) Epimerization of amine adduct of t⁶A. Synthetic ct⁶A epimers and *E. coli* total RNA were incubated with Tris buffer (pH 8.5) for 3 h. Nucleosides were analyzed by ODS/ESI-MS to detect Tris-adduct of t⁶A (*m/z* 516).

of N6 atom (163 ppm) of ct⁶A in ¹⁵N NMR implies the existence of hydantoin structure (Table 2). Second, the chemical shift of NH11 proton (9.72 ppm) of t⁶A moved toward high magnetic field by 1 ppm (8.72 ppm) in ct⁶A (Supplementary Figure S2), supporting the fact that hydrogen bond of NH11–N1 is impossible in the hydantoin isoform (Figure 1A). Third, two characteristic absorption bands at 1780 and 1730 cm⁻¹ in the IR spectrum of ct⁶A nucleoside (Supplementary Figure S1) also indicate carbonyl bond stretching in the hydantoin ring.

TcdA catalyzes ATP-dependent dehydration of t⁶A to form ct⁶A on tRNA (20). Given that TcdA is a ubiquitin-activating E1-like protein with ATPase activity, it is likely that it first adenylates the carboxyl group of t⁶A to form an activated ester intermediate, and subsequently allows the N6 nitrogen of t⁶A to attack the C13 carbon to cyclize the side chain with release of AMP. This reaction mechanism resembles the chemical synthesis of ct⁶A using a carbodiimide-type activating reagent such as EDC. Intriguingly, a previous study reported hydantoin ring formation of the t⁶A base using *N,N*-dicyclohexylcarbodiimide (DCC) (40). The activated ester intermediate of t⁶A with EDC or DCC is analogous to the adenylate intermediate of t⁶A generated by TcdA.

ct⁶A is easily hydrolyzed to convert to t⁶A under mild alkaline conditions (20). In addition, primary amines such as tris(hydroxymethyl)aminomethane or ethanolamine react efficiently with ct⁶A to generate amides of t⁶A (20,43,44). The hydantoin ct⁶A (Figure 1A) has two carbonyl carbons, C10 and C13, both of which could potentially be attacked by a water molecule or an amine. According to the general hydantoin chemistry, the non-ureido carbonyl carbon of a hydantoin compound is more susceptible to the reaction with nucleophiles, yielding the hydantoic acid and its derivatives (45–47). Thus, in the case of ct⁶A, C13 carbonyl carbon is naturally targeted by hydrolysis (20,40) and amine adduct formation (20,43,44), whereas the ureido C10 is comparatively non-reactive. In addition, we here showed that hydantoin ct⁶A is susceptible to epimerization under mild alkaline conditions, indicating that H12 in hydantoin ring is acidic enough for such process (48,49). It was shown that hydantoin derivatives are racemized as the result of tautomeric change (50). Just for 5 min incubation of L-ct⁶A at pH 9, 20–30% of L-ct⁶A is epimerized to yield D-*allo*-ct⁶A, and then it is hydrolyzed to form D-*allo*-t⁶A. The epimerization of ct⁶A and t⁶A also takes place at pH 8.2 under conventional nucleoside preparation (20). For tRNA preparation used for *in vitro* translation or other biochemical experiments, aminoacyl-moieties attached to 3' termini of aa-tRNAs isolated from the cell are frequently removed by mild alkaline treatment. According to the original methods, tRNA fractions extracted from the cell are incubated with 500 mM Tris-HCL (pH 8.8) (51) or 200 mM glycine buffer (pH 10.3) (52) for their deacylation. In these conditions, ct⁶A in tRNAs should be epimerized and converted to L-t⁶A and D-*allo*-t⁶A as well as Tris- and glycine-adducts of t⁶A, respectively. If D-*allo*-ct⁶A and D-*allo*-t⁶A have different activity in protein synthesis from their L-isomers, translational activity of tRNAs having ct⁶A should be reconsidered carefully. From these findings, we have learned that us-

age of primary amines and mild alkaline conditions should be avoided to handle and prepare tRNAs bearing ct⁶A.

As shown in the crystal structure of ct⁶A nucleoside, the hydantoin ring adopts a twisted position with a torsion angle of –52.7° against the adenine base (Figure 2A). From the *ab initio* energy calculation of hydantoin ring rotation, we identified four energy minimum rotamers with different η dihedral angles (127.3°, 67.3°, –52.7° and –122.7°) between the hydantoin and adenine rings (Figure 3). They all have ‘twisted conformation’ due to repulsive interaction between carbonyl oxygens of the hydantoin ring and the N1 and N7 nitrogens of the adenine moiety. In fact, actual conformation of ct⁶A in the crystal structure adopts one of these energy minimum rotamers. Although we do not have any experimental evidence to determine the orientation of the rings in solution, it is quite natural to assume that ct⁶A adopts ‘twisted conformation’ in solution, because repulsive interaction between the two rings should come from very basic chemical nature of ct⁶A. Strong rotational barriers (23 and 17.7 kcal) of the planar arrangement of the two rings of ct⁶A (Figure 3) restrict free rotation of C6–N6 bond. However, given that these barriers can be overcome by heat energy at normal growth temperatures, the hydantoin ring might be able to rotate to some extent under physiological conditions.

As observed in the crystal structure of the t⁶A37-containing anticodon stem-loop recognizing the AAG codon at the ribosomal A site (16), the N1–NH11 hydrogen bond extends a planar adenine base that stabilizes codon–anticodon pairing as well as the anticodon stem-loop structure. One possible structural model of the oxazolone ct⁶A (20) indicated that the oxazolone ring favors being fixed at the planar position with the adenine base to extend its π -conjugated system, enabling a strong stacking interaction with the codon–anticodon helix. This model provides a potential molecular basis for the contribution of ct⁶A to recognition of the adenine base of the ANN codon. However, the hydantoin ring of ct⁶A cannot adopt a planar position with the adenine base due to strong coulombic repulsion between the two rings. If there is no conformational restriction in the decoding center, the hydantoin ct⁶A may adopt one of the four twisted conformations on the ribosome. Taking account of the twisted conformation and low probability of π – π stacking of the hydantoin ring, it is an enigmatic issue how the twisted hydantoin ring stabilizes codon–anticodon interaction at the ribosomal A-site. Structural studies of 70S ribosome complexed with tRNA with ct⁶A37 and its cognate codon will be required to reveal the actual conformation of the hydantoin ring at the decoding center.

We here confirmed that the hydantoin isoform of ct⁶A is present in *E. coli* tRNAs. Presumably, this isoform is present in tRNAs from other organisms. However, we cannot rule out the possibility that the oxazolone isoform of ct⁶A may serve as an intermediate of the hydantoin isoform during biogenesis of ct⁶A.

AVAILABILITY

Crystallographic data (excluding structure factors) for the structures reported herein, have been deposited with the Cambridge Crystallographic Data Centre under accession

number CCDC 1458975. Copies of the data can be obtained free of charge at <http://www.ccdc.cam.ac.uk/>.

SUPPLEMENTARY DATA

Supplementary Data are available at NAR Online.

ACKNOWLEDGEMENTS

We are grateful to all members of the Sochacka and Suzuki laboratories for their technical support and many insightful discussions.

FUNDING

National Science Centre in Poland [UMO-2014/13/N/ST5/01591 to M.M.]; Grants-in-Aid for Scientific Research on Priority Areas from the Ministry of Education, Science, Sports and Culture of Japan (to T.S.). Funding for open access charge: Grants-in-Aid for Scientific Research on Priority Areas from the Ministry of Education, Science, Sports, and Culture of Japan.

Conflict of interest statement. None declared.

REFERENCES

- Machnicka, M.A., Milanowska, K., Osman Oglou, O., Purta, E., Kurkowska, M., Olchowik, A., Januszewski, W., Kalinowski, S., Dunin-Horkawicz, S., Rother, K.M. *et al.* (2013) MODOMICS: a database of RNA modification pathways—2013 update. *Nucleic Acids Res.*, **41**, D262–D267.
- Bjork, G. (1995) In: Soll, D and RajBhandary, UL (eds). *tRNA: Structure, Biosynthesis, and Function*. American Society for Microbiology, Washington, D.C., pp. 165–205.
- Grosjean, H. (2009) In: Grosjean, H (ed). *DNA and RNA Modification Enzymes: Structure, Mechanism, Function and Evolution*. Landes Bioscience, Austin, pp. 1–18.
- Suzuki, T. (2005) In: Grosjean, H (ed). *Fine-Tuning of RNA Functions by Modification and Editing*. Springer-Verlag Berlin and Heidelberg GmbH & Co. KG, Vol. **12**, pp. 23–69.
- Helm, M. and Alfonzo, J.D. (2014) Posttranscriptional RNA modifications: playing metabolic games in a cell's chemical Legoland. *Chem. Biol.*, **21**, 174–185.
- Agris, P.F., Vendex, F.A. and Graham, W.D. (2007) tRNA's wobble decoding of the genome: 40 years of modification. *J. Mol. Biol.*, **366**, 1–13.
- Yokoyama, S. and Nishimura, S. (1995) In: Soll, D and RajBhandary, UL (eds). *tRNA: Structure, Biosynthesis, and Function*. American Society for Microbiology, Washington, D.C., pp. 207–224.
- El Yacoubi, B., Bailly, M. and de Crécy-Lagard, V. (2012) Biosynthesis and function of posttranscriptional modifications of transfer RNAs. *Annu. Rev. Genet.*, **46**, 69–95.
- Gustilo, E.M., Vendex, F.A. and Agris, P.F. (2008) tRNA's modifications bring order to gene expression. *Curr. Opin. Microbiol.*, **11**, 134–140.
- Schweizer, M.P., Chheda, G.B., Baczynskyj, L. and Hall, R.H. (1969) Aminoacyl nucleosides. VII. N-(Purin-6-ylcarbamoyl)threonine. A new component of transfer ribonucleic acid. *Biochemistry*, **8**, 3283–3289.
- Niimi, T., Nureki, O., Yokogawa, T., Hayashi, N., Nishikawa, K., Watanabe, K. and Yokoyama, S. (1994) Recognition of the anticodon loop of tRNA(Ile) by isoleucyl-transfer-RNA synthetase from *Escherichia coli*. *Nucleos. Nucleot. Nucl.*, **13**, 1231–1237.
- Yarian, C., Townsend, H., Czestkowski, W., Sochacka, E., Malkiewicz, A.J., Guenther, R., Miskiewicz, A. and Agris, P.F. (2002) Accurate translation of the genetic code depends on tRNA modified nucleosides. *J. Biol. Chem.*, **277**, 16391–16395.
- Phelps, S.S., Malkiewicz, A., Agris, P.F. and Joseph, S. (2004) Modified nucleotides in tRNA(Lys) and tRNA(Val) are important for translocation. *J. Mol. Biol.*, **338**, 439–444.
- El Yacoubi, B., Hatin, I., Deutsch, C., Kahveci, T., Rousset, J.P., Iwata-Reuyl, D., Murzin, A.G. and de Crécy-Lagard, V. (2011) A role for the universal Kae1/Qri7/YgiD (COG0533) family in tRNA modification. *EMBO J.*, **30**, 882–893.
- Lin, C.A., Ellis, S.R. and True, H.L. (2010) The Sua5 protein is essential for normal translational regulation in yeast. *Mol. Cell. Biol.*, **30**, 354–363.
- Murphy, F.V., Ramakrishnan, V., Malkiewicz, A. and Agris, P.F. (2004) The role of modifications in codon discrimination by tRNA(Lys)UUU. *Nat. Struct. Mol. Biol.*, **11**, 1186–1191.
- Stuart, J.W., Gdaniec, Z., Guenther, R., Marszalek, M., Sochacka, E., Malkiewicz, A. and Agris, P.F. (2000) Functional anticodon architecture of human tRNA^{Lys}3 includes disruption of intraloop hydrogen bonding by the naturally occurring amino acid modification, t6A. *Biochemistry*, **39**, 13396–13404.
- Durant, P.C., Bajji, A.C., Sundaram, M., Kumar, R.K. and Davis, D.R. (2005) Structural effects of hypermodified nucleosides in the *Escherichia coli* and human tRNA^{Lys} anticodon loop: the effect of nucleosides s2U, mcm5U, mcm5s2U, mnm5s2U, t6A, and ms2t6A. *Biochemistry*, **44**, 8078–8089.
- Lescrinier, E., Nauwelaerts, K., Zanier, K., Poesen, K., Sattler, M. and Herdewijn, P. (2006) The naturally occurring N6-threonyl adenine in anticodon loop of *Schizosaccharomyces pombe* tRNA^I causes formation of a unique U-turn motif. *Nucleic Acids Res.*, **34**, 2878–2886.
- Miyauchi, K., Kimura, S. and Suzuki, T. (2013) A cyclic form of N6-threonylcarbamoyladenine as a widely distributed tRNA hypermodification. *Nat. Chem. Biol.*, **9**, 105–111.
- Crain, P.F. (1990) Preparation and enzymatic hydrolysis of DNA and RNA for mass spectrometry. *Methods Enzymol.*, **193**, 782–790.
- Kim, S., Lee, H. and Park, S. (2015) The structure of *Escherichia coli* TcdA (also known as CsdL) reveals a novel topology and provides insight into the tRNA binding surface required for N(6)-threonylcarbamoyladenine dehydratase activity. *J. Mol. Biol.*, **427**, 3074–3085.
- Lopez-Esteva, M., Arda, A., Savko, M., Round, A., Shepard, W.E., Bruix, M., Coll, M., Fernandez, F.J., Jimenez-Barbero, J. and Vega, M.C. (2015) The crystal structure and small-angle X-ray analysis of CsdL/TcdA reveal a new tRNA binding motif in the MoeB/E1 superfamily. *PLoS One*, **10**, e0118606.
- Matuszewski, M. and Sochacka, E. (2014) Stability studies on the newly discovered cyclic form of tRNA N(6)-threonylcarbamoyladenine (ct(6)A). *Bioorg. Med. Chem. Lett.*, **24**, 2703–2706.
- Chheda, G. and Hong, C.I. (1971) Synthesis of naturally occurring 6-ureidopurines and their nucleosides. *J. Med. Chem.*, **14**, 748–753.
- Hong, C.I. and Chheda, G.B. (1972) In: Townsend, L.B. and Tipson, R.S. (eds). *Nucleic Acid Chemistry*. John Wiley & Sons, NY, pp. 661–664.
- Hong, C.I., Chheda, G.B., Dutta, S.P., O'Grady-Curtis, A. and Tritsch, G.L. (1973) Synthesis and biological activity of analogs of naturally occurring 6-ureidopurines and their nucleosides. *J. Med. Chem.*, **16**, 139–147.
- Adamiak, R.W. and Wiewiórowski, M. (1975) The modified nucleosides of tRNAs. Synthesis and spectra of some natural ureidonucleosides. *Bull. Acad. Pol. Sci., Ser. Sci. Chim.*, **23**, 241–253.
- Martin, D. and Schlimme, E. (1994) Preparation of ureidonucleosides of the threonine isomers. *Z. Naturforsch. C*, **49**, 834–842.
- Allen, F.H. (2002) The Cambridge Structural Database: a quarter of a million crystal structures and rising. *Acta Crystallogr., Sect. B: Struct. Sci.*, **58**, 380–388.
- Sakaguchi, Y., Miyauchi, K., Kang, B.I. and Suzuki, T. (2015) Nucleoside analysis by hydrophilic interaction liquid chromatography coupled with mass spectrometry. *Methods Enzymol.*, **560**, 19–28.
- Suzuki, T., Ikeuchi, Y., Noma, A., Suzuki, T. and Sakaguchi, Y. (2007) Mass spectrometric identification and characterization of RNA-modifying enzymes. *Methods Enzymol.*, **425**, 211–229.
- Arico, J.W., Calhoun, A.K., Salandria, K.J. and McLaughlin, L.W. (2010) Tetramethylsuccinimide as a directing/protecting group in purine glycosylations. *Org. Lett.*, **12**, 120–122.
- Parthasarathy, R., Ohrt, J.M. and Chheda, G.B. (1974) Conformation and possible role of hypermodified nucleosides adjacent to 3'-end of anticodon in tRNA: N-(purin-6-ylcarbamoyl)-L-threonine riboside. *Biochem. Biophys. Res. Commun.*, **60**, 211–218.

35. Parthasarathy,R., Ohrt,J.M. and Chheda,G.B. (1977) Modified nucleosides and conformation of anticodon loops: crystal structure of t6A and g6A. *Biochemistry*, **16**, 4999–5008.
36. Altona,C. and Sundaralingam,M. (1972) Conformational analysis of the sugar ring in nucleosides and nucleotides. A new description using the concept of pseudorotation. *J. Am. Chem. Soc.*, **94**, 8205–8212.
37. Saenger,W. (1984) *Principles of Nucleic Acids Structure*. Springer: NY.
38. Buchman,R. and Komoroski,R.A. (1980) A carbon-13 and nitrogen-15 NMR study of some nitrogen heterocycles. *J. Heterocycl. Chem.*, **17**, 1089–1092.
39. Westerman,P.W., Botto,R.E. and Roberts,J.D. (1978) Substituent and medium effects on Nitrogen-15 shieldings of compounds with >C=N bonds (imines, oximes and phenylhydrazones). *J. Org. Chem.*, **43**, 2590–2596.
40. Hong,C.I. and Chheda,G.B. (1975) Purinylhydantoins. Facile conversion of the naturally occurring N-(purin-6-ylcarbamoyl)-L-amino acids into 3-purin-6-ylhydantoins and 3-cyclohexyl-1-(purin-6-ylcarbamoyl)hydantoins. *J. Med. Chem.*, **18**, 79–84.
41. Rosemeyer,H., Toth,G., Golankiewicz,B., Kazimierzczuk,Z., Bourgeois,W., Kretschmer,U., Muth,H.P. and Seela,F. (1990) *Syn-anti* conformational analysis of regular and modified nucleosides by 1D 1H NOE difference spectroscopy: a simple graphical method based on conformationally rigid molecules. *J. Org. Chem.*, **55**, 5784–5790.
42. Lynch,S.R. and Tinoco,I. Jr (1998) The structure of the L3 loop from the hepatitis delta virus ribozyme: a syn cytidine. *Nucleic Acids Res.*, **26**, 980–987.
43. Nishimura,S. (1972) Minor components in transfer RNA: their characterization, location, and function. *Prog. Nucleic Acid Res. Mol. Biol.*, **12**, 49–85.
44. Kasai,H., Murao,K., Nishimura,S., Liehr,J.G., Crain,P.F. and McCloskey,J.A. (1976) Structure determination of a modified nucleoside isolated from *Escherichia-coli* transfer ribonucleic-acid - N-(N-(9-beta-D-ribofuranosylpurin-6-Yl)carbamoyl)threonyl)2-amido-2-hydroxymethylpropane-1,3-diol. *Eur. J. Biochem.*, **69**, 435–444.
45. Blagoeva,I.B., Pojarlieff,I.G. and Dimitrov,V.S. (1978) Alkaline-hydrolysis of hydantoin, 3-methylhydantoin, and 1-acetyl-3-methylurea - effect of ring size on cleavage of acylureas. *J. Chem. Soc., Perkin Trans. 2*, 887–892.
46. Meusel,M. and Gutschow,M. (2004) Recent developments in hydantoin chemistry – a review. *Org. Prep. Proced. Int.*, **36**, 391–443.
47. Lopez,C.A. and Trigo,G.G. (1985) The chemistry of hydantoins. *Adv. Heterocycl. Chem.*, **38**, 177–228.
48. Dudley,K.H. and Bius,D.L. (1976) Buffer catalysis of the racemization reaction of some 5-phenylhydantoins and its relation to the in vivo metabolism of ethotoin. *Drug Metab. Dispos.*, **4**, 340–348.
49. Lazarus,R.A. (1990) Chemical racemization of 5-benzylhydantoin. *J. Org. Chem.*, **55**, 4755–4757.
50. Dakin,H.D. (1910) The catalytic racemization of optically active hydantoin derivatives and of related substances as the result of tautomeric change. *Am. Chem. J.*, **44**, 48–60.
51. Von Ehrenstein,G. and Lipmann,F. (1961) Experiments on hemoglobin biosynthesis. *Proc. Natl. Acad. Sci. U.S.A.*, **47**, 941–950.
52. Zubay,G. (1962) The isolation and fractionation of soluble ribonucleic acid. *J. Mol. Biol.*, **4**, 347–356.